

Experimental Study for μ -class Control of Relative Position and Attitude for Synthetic Aperture Telescope Using Formation Flying Micro-satellites

Ryo Suzumoto* Satoshi Ikari* Norihide Miyamura**
Shinichi Nakasuka*

* *Department of Aeronautics and Astronautics, The University of
Tokyo, Tokyo, Japan (e-mail: suzumoto@space.t.u-tokyo.ac.jp,
ikari@space.t.u-tokyo.ac.jp, nakasuka@space.t.u-tokyo.ac.jp).*

** *School of Science and Engineering, Meisei University, Tokyo, Japan
(e-mail: norihide.miyamura@meisei-u.ac.jp)*

Abstract: Earth remote sensing from geostationary orbit (GEO) realizes high time resolution that is essential for disaster monitoring; however, the spatial resolution is commonly worse than observation from low Earth orbit (LEO). In order to achieve high-resolution and high-frequency GEO remote sensing, we have proposed a “Formation Flying Synthetic Aperture Telescope (FFSAT)” with multiple micro-satellites. The FFSAT can improve the spatial resolution by using the technique of a synthetic aperture, and therefore the relative positions and attitudes between the optical units of each satellite must be controlled with an accuracy better than $1/10$ of the observation wavelength. In order to verify feasibility of such highly accurate control, μ -class control experiments were conducted by using COTS components, and numerical models of the components were constructed. Results of the experiments were integrated into a software simulator, and the μ -class formation flying control of the entire FFSAT system was numerically evaluated. In this simulation, highly accurate control was achieved with dual-stage actuators, which consist of piezo actuators and thrusters. The simulation results show that the formation can be controlled in μ -class accuracy under some assumptions.

Keywords: Micro-Satellites, Relative Position and Attitude Control, Formation Flying, Synthetic Aperture Telescope, GEO Remote Sensing, Numerical Modeling

1. INTRODUCTION

Disaster monitoring by Earth observation satellites is a valuable information source to obtain wide-area ground situations at one time. Spatial resolution (image resolution) and observation frequency (temporal resolution) are also important for Earth observation. Geostationary orbit (GEO) remote sensing that places an Earth observation satellite on GEO can realize high-frequency observation on minute order; however because of its high altitude, it has the disadvantage that it is difficult to obtain high resolution compared to observation from low Earth orbit (LEO). In order to improve the resolution, there is no other way to increase the aperture of the optical system. However due to the restrictions such as a size of a launch vehicle or development cost, it is difficult to arrange a huge optical system in GEO. As a technique to reach high resolution without using a huge structure, a synthetic aperture telescope has been studied. The method obtains a virtual large aperture by arranging small sub-apertures that are interferometrically combined to achieve a resolution comparable to a primary aperture equivalent to the entire array size. As a space telescope, a synthetic aperture telescope realized by satellite formation flying such as TPF mission (Scharf et al. (2004)) has been proposed. It can

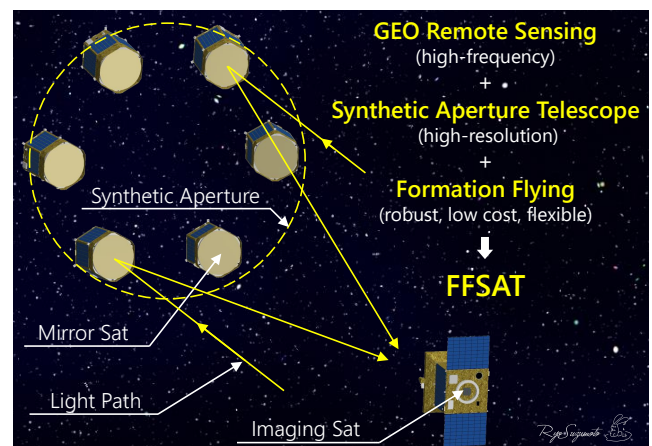


Fig. 1. Concept image of the FFSAT. In this figure, 6 mirror satellites form a virtual large mirror, which is focused on an imaging satellite.

realize a large aperture which is not comparable to that of a single satellite and can attain a high resolution which could not be achieved until now.

We have proposed to use a synthetic aperture telescope with formation flying multiple micro-satellites for the

Table 1. Requirements of the FFSAT for the forest fire monitoring mission.

	Unit	Value
GSD	m	30
Field of view	km×km	1,000 × 1,000
Observation frequency	min	10
Orbital altitude	km	35,786 (GEO)
Observation wavelength	μm	4 (infrared)
Focal length	m	21.5
Synthetic aperture diameter	m	5.82
Required piston control accuracy	nm	400
Required tilt control accuracy	prad	0.42

GEO remote sensing called “Formation Flying Synthetic Aperture Telescope (FFSAT)” as a method to realize high-resolution and high-frequency observation (Fig. 1). Furthermore, we have considered the Australian forest fire monitoring mission as the first practical application of the FFSAT. In previous projects, satellites Terra and Aqua equipped with NASA’s visible/infrared radiometer MODIS, which achieved 1 km ground sample distance (GSD) from the altitude of 705 km, and they can observe a same point in one to two days cycle (Hutchison (2003)). By contrast, in the FFSAT preliminarily designed by us (Suzumoto et al. (2019)), it is possible to achieve both high-resolution observation of 30 m GSD and high-frequency observation in 10 minutes order in infrared ray (See Table 1).

The FFSAT can achieve both high-resolution observation and high-frequency observation. However, in order to realize the FFSAT, it is necessary to determine and control the relative positions and attitudes with an accuracy better than 1/10 of the observation wavelength (e.g., in the case of infrared ray, 0.1 μm order) (Rousset et al. (2001)), which is extremely high-accuracy and not comparable to the conventional satellite control. Fig. 2 shows the relative position control accuracy of formation flyings and related technologies. The area surrounded by the blue dashed line is already demonstrated on orbit. As for a nano- and micro-satellite formation flying, CanX-4&5 mission have succeeded in formation control to an accuracy of 1 m (Bandyopadhyay et al. (2016)). In recent years, formation flying mission projects with cm-class accuracy such as mDOT (D’Amico et al. (2019)) are proposed, which are included in the area surrounded by the red dashed line. By contrast, the required control accuracy of the FFSAT is 0.1 μm order, which is incomparably high as shown in Fig. 2. Fig. 3 summarizes the accuracy and operation range of sensors and actuators, which are commercial off-the-shelf (COTS) products and small enough to be installed for micro-satellites. High-precision thrusters such as cold gas thrusters and colloid thrusters are being developed (Armano et al. (2019)), but they do not reach the required accuracy of the FFSAT. To overcome the accuracy limits of thrusters, more precise device like piezo stages (PZS) can be useful. ASTERIA (Smith et al. (2018)) has achieved great pointing accuracy of 2.4 μrad/20 minutes (1σ) using a satellite attitude control system in combination with PZSs. A deformable mirror used in the field of optical compensation can drive a mirror surface with an accuracy of less than the wavelength order, and DeMi (Holden et al. (2019)) will be launched soon in order to demonstrate a deformable mirror on orbit. Highly accurate relative position and attitude estimation among satellites can be

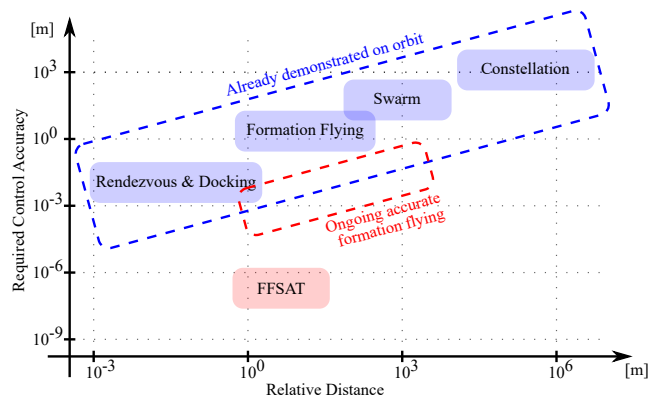


Fig. 2. Comparison with related technologies.

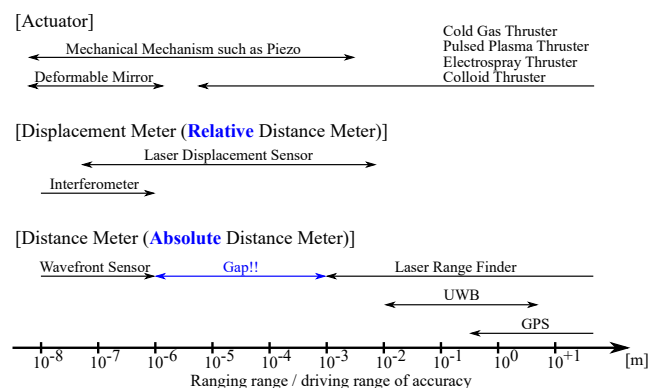


Fig. 3. Accuracy and operation range of sensors and actuators available for micro-satellites.

achieved by accurately measuring the distance between multiple points of satellites. However, there is no absolute distance meter in the range marked “Gap” in Fig. 3.

We have already conducted some studies to realize formation flying with an accuracy of 1/10 of the observation wavelength. In order to fill the gap of the absolute distance meter shown in Fig. 3 and construct an ultra-high-accuracy formation flying for the FFSAT, we have proposed a method called “PSF optimization method” (Suzumoto et al. (2019)). In this method, a captured point light source image by the FFSAT is optimized while observing the relative position and attitude displacement between satellites with high-precision displacement sensors. Consequently, even if the absolute distance between satellites cannot be measured with high accuracy, an algorithm to construct an ultra-high-accuracy formation flying that can obtain an effective image was shown. In addition, by using deformable mirrors, we have proposed methods to improve the image quality at the edge of view, and to change the direction of the telescope without moving the center of gravity of the formation flying satellites (Miyamura et al. (2019)). However, in order to effectively use these methods and to make observations, it is necessary to keep the constructed or constructing formation with ultra-high accuracy. Therefore, a control law using multi-stage actuators composed of thrusters, PZSs, and deformable mirrors is required.

This paper focuses on the μm-class formation keeping. Based on observations with high-precision laser displacement sensors (LDS), the relative position and attitude among satellites could be controlled with μm-class accu-

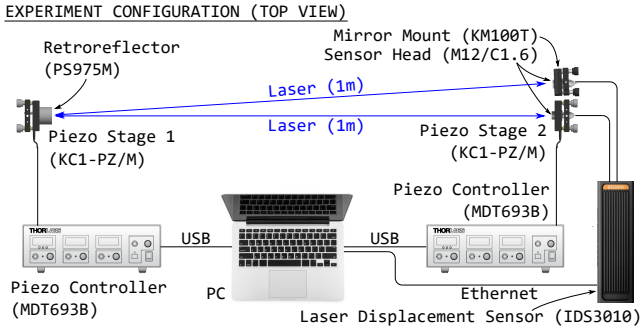


Fig. 4. Experimental configuration for numerical modeling of components and single-axis control experiment. All devices are installed on a vibration isolation table.

racy using dual-stage actuators, which consist of thrusters and PZSs. We used COTS components of LDSs and PZSs for control experiments to construct numerical models of the components. Results of the experiments were integrated into a software simulator, and the μm -class formation flying control of the entire FFSAT system was simulated. Please note that adaptive optics and deformable mirrors will be used for $0.1 \mu\text{m}$ -class control, but we will not deal with that in this paper.

2. MODELING OF THE COMPONENTS

A LDS and a PZS (in this case, both are not space qualified products) that are useful for μm -class control were evaluated and numerically modeled by experiments. In addition, a cold gas thruster and an absolute attitude determination system were also numerically modeled with reference to existing components.

2.1 Experimental Configuration

In order to construct numerical models of the components, performance evaluation experiments of a LDS and a PZS were conducted. We used attocube's LDS IDS3010 and Thorlabs' PZS KC1-PZ/M. Fig. 4 shows the experimental configuration. The model numbers of the devices are shown in parentheses. The displacement of the PZS 1 can be observed with two LDSs.

2.2 Evaluation of the Laser Displacement Sensor

The measurement accuracy was verified by measuring with two independent LDSs. Fig. 5 shows the measurement results when none of the PZSs were driven. It seems that disturbances which could not be removed by the vibration isolation table were observed (e.g., low-frequency ground vibration, air vibration, and thermal deformation). Ground vibration is almost eliminated, and the environment is sufficient for experiments with μm -class accuracy. Fig. 6 shows the measurement results when the PZS 1 was randomly walked. The random walk input signal d was generated by integrating the white Gaussian noise n as follows:

$$d(t + \Delta t) = d(t) + n(t) \quad (1)$$

where n is white Gaussian noise with a standard deviation of 3 V which is equivalent to about $0.15 \mu\text{m}$ in the drive amount of the PZS, t is time, and Δt is a time interval of

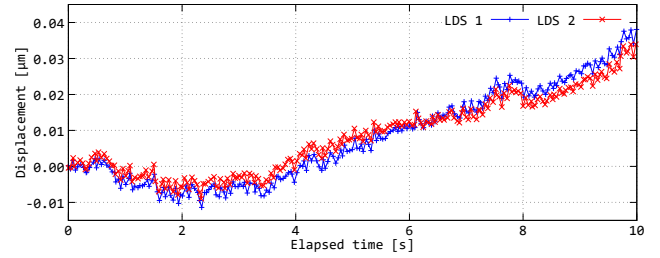


Fig. 5. Measurement results with the LDSs when the PZSs were not driven.

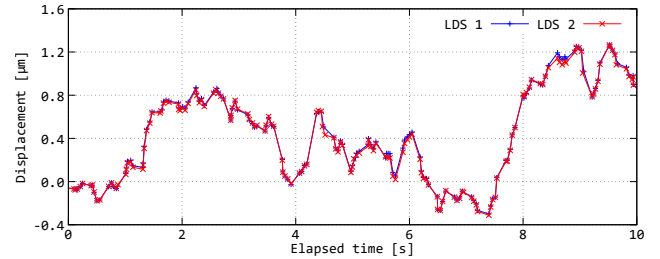


Fig. 6. Measurement results with the LDSs when the PZS 1 was randomly walked.

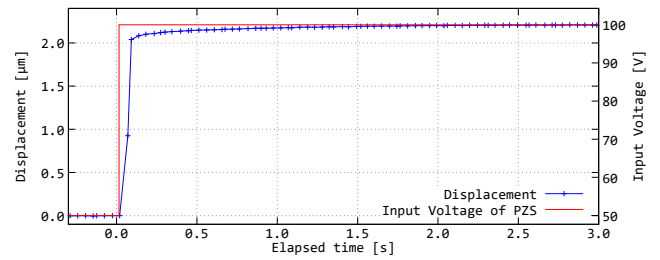


Fig. 7. Step response of the PZS (Experimental result).

signal input. In this experiment, Δt was set $1/55$ seconds. From these figures, it was confirmed that the LDSs have a measurement reproducibility of at least 10 nm . The maximum measurement frequency via Ethernet was about 25 Hz .

2.3 Evaluation of the Piezo Stage

The PZS was evaluated by driving the PZS 1 and measuring with the LDS. The maximum control frequency was about 55 Hz when using the piezo controller via USB. The measured step response is shown in Fig. 7. It can be found that the response delay is approximately 0.07 seconds. However, it should be noted that this delay is not all caused by the PZS, but includes all of the delays due to the LDS, the PZS itself, and the piezo controller. Fig. 8 and 9 show the response when the input voltage was changed stepwise and randomly walked respectively. These figures show hysteresis in the movement of the PZS.

The modeling of this hysteresis was considered. The Bouc-Wen model is a hysteresis model which can be described by differential equations with a small number of parameters. Tatebatake et al. (2017) have proposed an improved Bouc-Wen model represented as following equations

$$\begin{cases} y = A_1 x - h \\ \dot{h} = A \dot{x}(t) + A_0 |\dot{x}(t)| - \gamma \dot{x}(t) |h|^n - \beta |\dot{x}(t)| |h|^{n-1} h \end{cases} \quad (2)$$

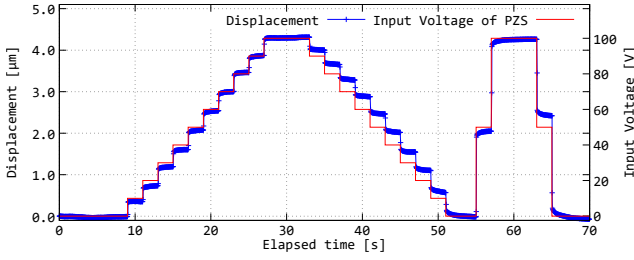


Fig. 8. Hysteresis of the PZS (Experimental result).

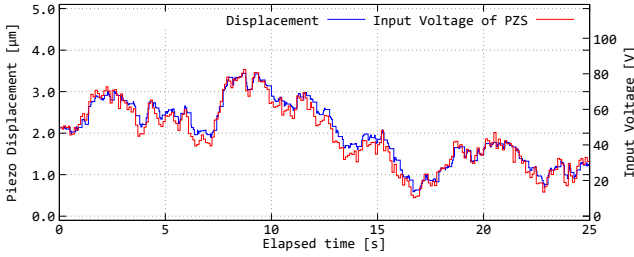


Fig. 9. Response of the PZS to random walk input (Experimental result).

where x is input, y is output, h is a hysteresis component, and $A, A_0, \beta, \gamma,$ and n are parameters. The improved Bouc–Wen model can well express the measured hysteresis in the case of sin input response which reciprocated over the entire output width of the PZS. However, in the FFSAT, it is assumed that the PZS is moved in small increments in order to remove the control error by the thrusters. In this case, the input and output gradually separated as shown in Fig. 10. Therefore, this model was modified as follows:

$$\begin{cases} x = \mathcal{R}_{\text{emap}}\{u\}_{[\text{Input voltage range}] }^{[-1,1]} \\ z = \mathcal{R}_{\text{emap}}^{-1}\{y\}_{[\text{Piezo output range}] }^{[-1,1]} \\ y = A_1x - h + d \\ \dot{h} = A\dot{x}(t) + A_0|\dot{x}(t)| - \gamma\dot{x}(t)|h|^n - \beta|\dot{x}(t)||h|^{n-1}h \\ \dot{d} = -\frac{\alpha}{dt}((A_1x - h + d) - x) \end{cases} \quad (3)$$

where u is input, z is output, and α is an additional parameter. The values differ greatly between input and output. In other words, the voltage input is on the order of 10 V, while the displacement output is on the order of μm . Therefore, in order to stabilize the numerical calculation, the input and output values are normalized by the $\mathcal{R}_{\text{emap}}\{\cdot\}_{[\text{from}]}^{[\text{to}]}$ function, which is defined as a linear transformation from interval [from] to interval [to]. The experimental results in Fig. 8 and 9 were reproduced by this our modified Bouc–Wen model, and Fig. 11 and 12 show the results. These results show that the hysteresis is well modeled.

2.4 Modeling of the Cold Gas Thruster

A cold gas thruster installed on ESA’s LISA Pathfinder is one of the thrusters that can control thrust with high precision and has already been demonstrated on orbit (Gath et al. (2004); Armano et al. (2019)). We simulated the power spectral density (PSD) of the required noise level of the LISA Pathfinder’s thruster as follow:

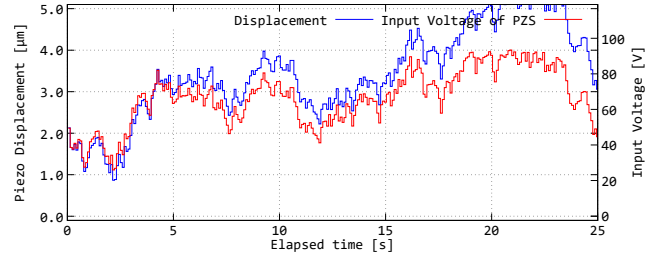


Fig. 10. Response of the PZS to random walk input (Simulation by improved Bouc–Wen model).

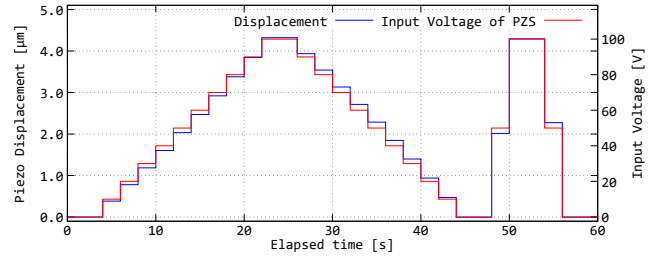


Fig. 11. Hysteresis of the PZS (Simulation by our modified Bouc–Wen model).

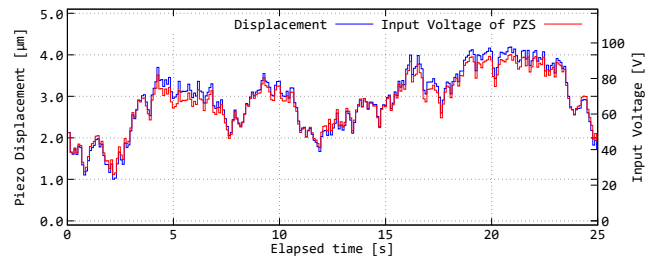


Fig. 12. Response of the PZS to random walk input (Simulation by our modified Bouc–Wen model).

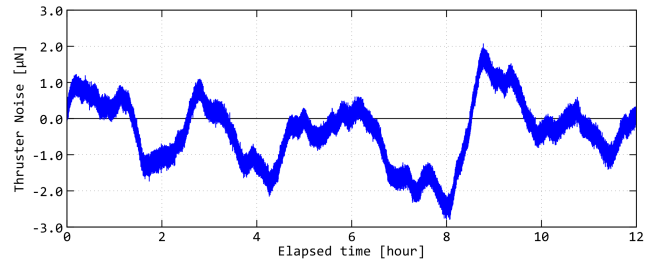


Fig. 13. Noise model of the thruster. The time series data of the noise generated from the noise shape of Fig. 14.

$$G(s) = 10^{-7} \times \left(\frac{s + 2\pi \times 6.0 \times 10^{-3}}{s + 2\pi \times 1.5 \times 10^{-4}} \right)^2 \quad (4)$$

Fig. 13 shows the time series noise data generated from (4). Fig. 14 shows the PSD calculated from this data and the transfer function of the noise model. It was confirmed that the noise equivalent to the requirement of LISA Pathfinder’s thruster was generated. This noise model has an error of about $0.2 \mu\text{N}$ in the short term and an offset of about $1 \mu\text{N}$ in the long term.

2.5 Modeling of the Absolute Attitude Determination System

The observation quantities required for the control of the formation flying are the relative position and attitude.

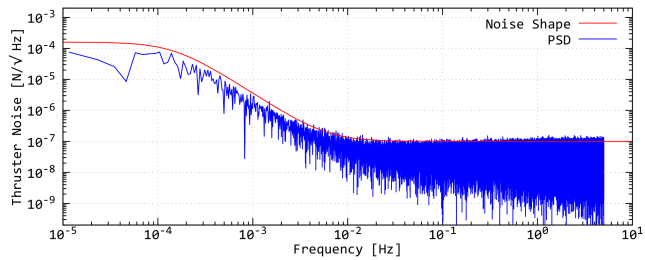


Fig. 14. Noise model of the thruster. Noise shape of (4) and PSD calculated from the data in Fig. 13.

However, an absolute attitude sensor is also indispensable for the FFSAT to point to the desired position on the ground. The attitude determination system combining star trackers (STT) and fibre-optic gyroscopes (FOG) can determine the attitude with high accuracy while estimating the random drift of FOGs. STTs for micro-satellites with attitude determination accuracy of about 5 arcsec are commercially available. Based on the current situation, the attitude determination system is assumed to be able to estimate the absolute attitude with an accuracy of $10 \mu\text{rad}$ (1σ), and the determination error is assumed to be white Gaussian noise.

3. CONTROL EXPERIMENTS AND VALIDATION OF THE NUMERICAL MODELS

Single-axis and 3-axis hardware control experiments were performed. In addition, the hardware experiments were emulated in software simulation. From the results, the validity of the numerical models was confirmed, and it was shown that control with an accuracy of μm order or less is possible.

3.1 Single-axis Control Experiment and Emulation

Experimental configuration The experimental configuration is the same as in Fig. 4. The PZS 1 was used for disturbance input (hereinafter “Dist-PZS”), and the PZS 2 was used for control (hereinafter “Ctrl-PZS”). A disturbance was applied to the Dist-PZS, and the displacement was measured with a LDS attached to the Ctrl-PZS. The Ctrl-PZS was PD-controlled to keep the distance between the two PZSs constant. A random walk signal was added to the Dist-PZS, which is the same as in (1). The control frequency of the Ctrl-PZS was 20 Hz. Although not used for control, a LDS was attached to the mirror mount to measure the displacement of the Dist-PZS independently.

Control result A control result is shown in Fig. 15. In the top figure, the red line shows the driving amount of the Dist-PZS, and the blue line shows the displacement between the two PZSs. In the bottom figure, the blue line shows the input voltage of Dist-PZS and the red line shows that of the Ctrl-PZS. The Dist-PZS was driven after 5 seconds, and the Ctrl-PZS was driven after 15 seconds. Since the directions of the two PZSs are opposite, the input voltage to the Ctrl-PZS is inverted at 50 V. From the figure, it was found that the displacement converges around 0 after the start of the control, and the distance between the PZSs can be controlled with an accuracy of $0.47 \mu\text{m}$ (3σ) although high-frequency components cannot

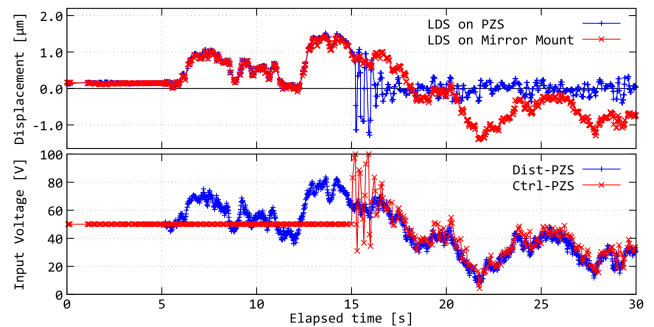


Fig. 15. Results of the single-axis control experiment.

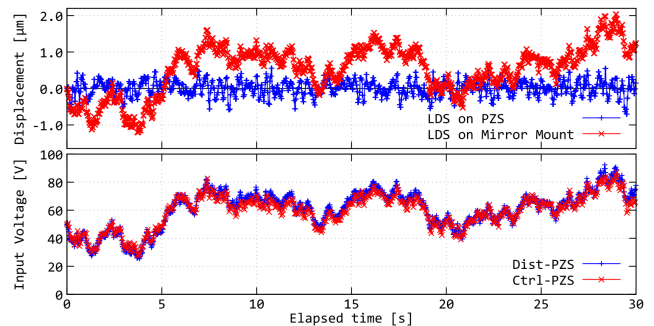


Fig. 16. Emulation results of the single-axis control experiment (Fig. 15) in the software simulation.

Table 2. Settings of the emulation of the single-axis control experiment.

	Unit	Value
Measured value update frequency of the LDS	Hz	25
Driving frequency of the Dist-PZS	Hz	50
Response delay of the PZS	s	0.07
Control frequency	Hz	20
Hysteresis model of the PZS	-	Eq. (3)

be removed due to the response delay of the PZS mentioned in Section 2.3. Besides, the bottom Fig. 15 shows that the Ctrl-PZS can follow the Dist-PZS. Since the control accuracy of $0.47 \mu\text{m}$ is smaller than the assumed observation wavelength of $4 \mu\text{m}$, this error can be removed by adaptive optics using deformable mirrors.

Emulation in software simulation In order to confirm the validity of the numerical models, the hardware experiment was emulated by software simulation. Table 2 shows the settings of the software simulation, using the numerical models constructed in Section 2. The emulation result is shown in Fig. 16. The hardware experiment can be almost reproduced except that the control accuracy is slightly poor compared to Fig. 15.

3.2 3-axis Control Experiment and Emulation

Experimental configuration Fig. 17 shows the experimental configuration. 3-axis PZSs are installed on both the upper and lower sides. The upper side simulates an imaging satellite, and the lower side simulates a mirror satellite. Between the two satellites, three LDSs measure the displacements. In this experiment, three degrees of freedom of relative position (piston) and attitude (tip and tilt) between two satellites were controlled.

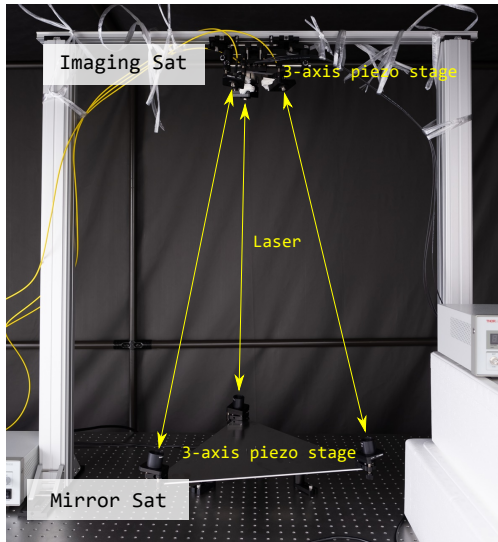


Fig. 17. Configuration for 3-axis control experiment.

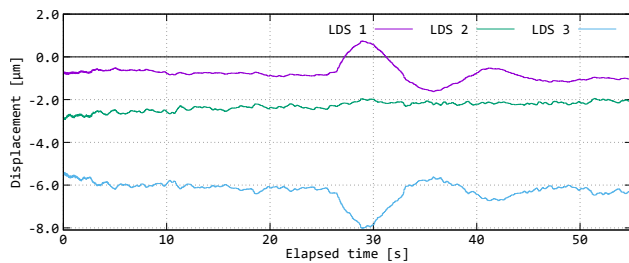


Fig. 18. Disturbance input for the 3-axis control experiment.

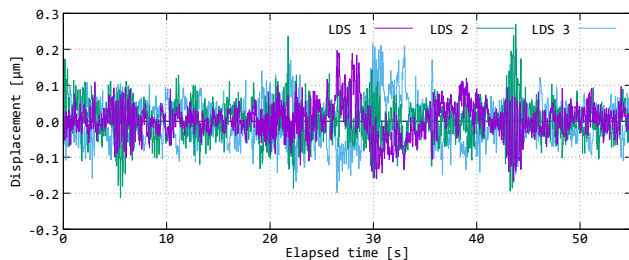


Fig. 19. Results of the 3-axis control experiment.

Control result in hardware experiment and emulation result in software simulation As a disturbance input of the experiment, a control error by the thrusters calculated by the simulator for the entire FFSAT system described in Section 4 was given to the PZS simulating an imaging satellite (Fig. 18). The PZS simulating a mirror satellite was PD-controlled so that the relative position and attitude between the two satellites were constant. The control result is shown in Fig. 19. The PZS eliminates the control error caused by the thrusters and achieves control accuracy of $0.17 \mu\text{m}$ (3σ), less than μm order. Besides, Fig. 20 shows the result of emulating this experiment in the software simulation, which is well reproduced.

From the emulation results of the single-axis and 3-axis experiments, the validity of the numerical models was confirmed.

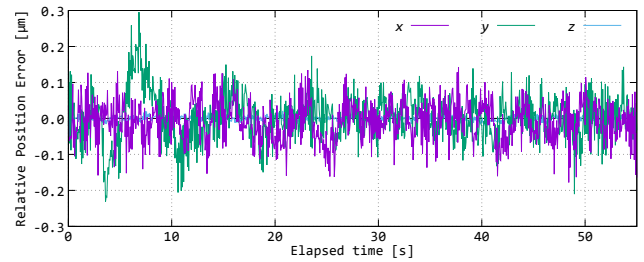


Fig. 20. Emulation results of 3-axis control experiment (Fig. 19) in the software simulation.

4. CONTROL OF THE ENTIRE FFSAT SYSTEM IN SOFTWARE SIMULATION INTEGRATING THE EXPERIMENTAL RESULTS

In the hardware experiments of the previous section, the control with single axis and 3 axis was verified. However, in the FFSAT currently under consideration, there are 7 satellites, and 6 axes of each position and attitude must be controlled with μm -class accuracy. Therefore, a software simulator that reflected the results in the hardware experiments was created, and the control of the entire FFSAT system was verified.

4.1 Specifications of simulation and models of components and disturbance

It is assumed that the STTs, the FOGs, the LDSs are installed as sensors, and the thrusters and the PZSs are installed as actuators. A reaction wheel (RW) is not installed because it is considered that the micro-vibrations caused by RWs adversely affect highly accurate control. Table 3 shows the specifications of the simulation.

Fig. 23 shows the determination and control dynamics of FFSAT. In the case of the imaging satellite, only the absolute attitude was controlled because the position of the imaging satellite is set as the origin of the formation coordinate and the absolute position of formation flying is not focused on in this simulation. All mirror satellites followed the imaging satellite to keep the relative position and attitude with respect to the imaging satellite. If the imaging satellite has a high control frequency and vibrates rapidly in a small width, it will be difficult for the mirror satellites to follow it. Accordingly, the control frequency of the imaging satellite was set low.

4.2 Simulation results and discussion

Fig. 24 shows simulation results. From the top figure, the position errors of the mirror satellites with respect to the imaging satellite, the attitude errors of the mirror satellites with respect to the imaging satellite, absolute attitude error of the imaging satellite, the control history of constant thrusters, that of control thrusters of mirror satellite 2, and that of control thrusters of imaging satellite are shown. At the beginning of the simulation, only the thrusters were used, and the PZSs were driven 10 minutes after the start of the simulation. By using high-precision thrusters, the relative position control accuracy of $1 \mu\text{m}$ and relative attitude control accuracy of $0.7 \mu\text{rad}$ were achieved. In addition, by driving the PZSs, it was possible to improve the relative position control accuracy to $0.3 \mu\text{m}$

Table 3. Specifications of the simulation for keeping the formation of the FFSAT.

SATELLITE	
Number	1 imaging satellite and 6 mirror satellites
Mass, Moment of inertia	50 kg-class. Use the value designed by us (Suzumoto et al. (2019)). The specs of the 6 mirror satellites were given a variation of 0.1 %.
ORBIT	
Coordinate	Local-Vertical-Local-Horizontal (LVLH) frame
Initial orbit	GEO at an east longitude of 140°
Formation	See Fig. 21
ORBITAL DISTURBANCE	
Geopotential	Up to third order
Third bodies	Sun, Moon
COMPONENT	
LDS	Fig. 22 shows the arrangement. The displacements can be measured with 100 nm accuracy (blue arrows in Fig. 22), and the positions of the laser receiving point can be measured with 1 μm accuracy (red arrows in Fig. 22).
STT & FOG	Absolute attitude estimation accuracy of 10 μrad (1σ). The noise model was white Gaussian noise.
PZS	Numerical model constructed in Section 2.3. 0.1 second response delay. Maximum stroke was 10 μm (position) and 10 μrad (attitude).
Thruster	Numerical model constructed in Section 2.4. Maximum thrust is 20 μN. All satellites had 12 control thrusters, 2 on each of 6 planes (±x, y, z), for highly accurate position and attitude control. In addition, there is one constant thruster to cancel the relative gravity disturbance derived from Hill's equation.
RW	Not installed
CONTROL	
Control law	PID control. The mirror satellites follow the imaging satellite.
Frequency	1/10 Hz for imaging satellite, 10 Hz for mirror satellites

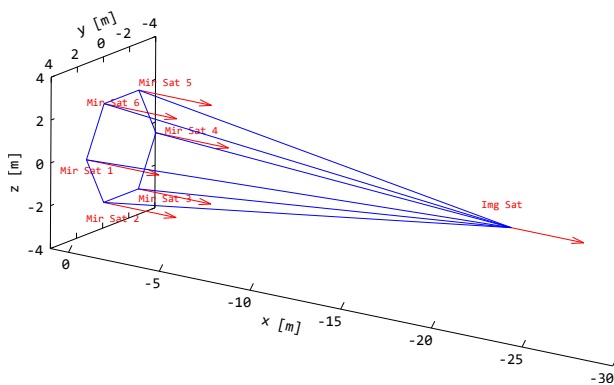


Fig. 21. Initial formation of the FFSAT. The origin is GEO at an east longitude of 140°. Satellites are placed at the intersection of the blue lines, and the red arrows indicate the satellites' z axis.

and the relative attitude control accuracy to 0.3 μrad. It was found that the μm-class control required to connect the control to adaptive optics using deformable mirrors can be achieved. Furthermore, the absolute positions were not controlled in this simulation. In the 24-hour simulation, the formation was drifted about 14 km in the y axis direction.



Fig. 22. Arrangement of LDSs.

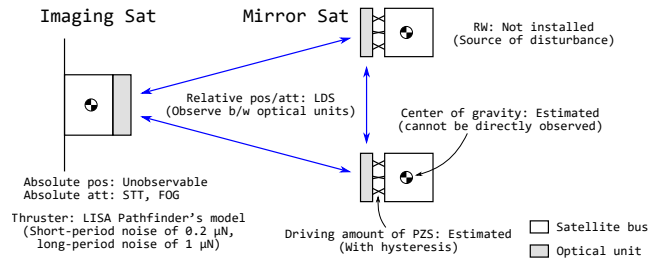


Fig. 23. Dynamics of the FFSAT.

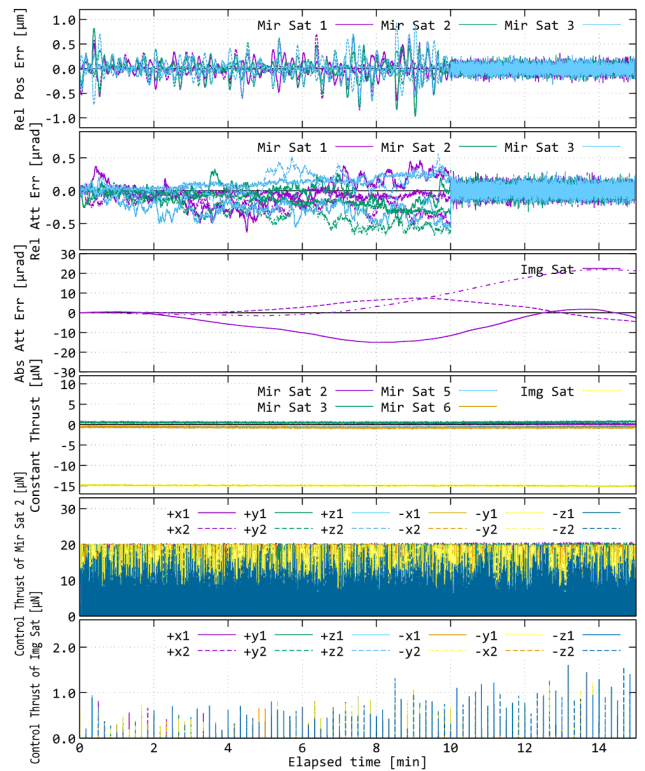


Fig. 24. Simulation results. In the control error graph, the solid lines, broken lines, and dash-dot lines represent the x, y, and z axes, respectively.

Because highly accurate control is required, the thrusters kept the relative position and attitude by continuously making thrust from each side. The necessary impulse of the mirror satellite 2 at the simulation was 62 μN s/s. In other words, the consumed fuel weight was about 2.8 kg/year, assuming cold gas thrusters with I_{sp} of 70 seconds. This is not a small value for micro-satellites, and a control law to reduce fuel is required.

5. CONCLUSION

In order to realize the “Formation Flying Synthetic Aperture Telescope (FFSAT)”, which has been proposed as a forest fire monitoring mission, the highly accurate formation keeping of μm -class was verified. To evaluate the feasibility of such accurate control, performance evaluation experiments using COTS components were conducted and characteristics of the components were numerically modeled. In the hardware experiment of single-axis control, the distance between two piezo stages (PZS) could be kept constant with an accuracy of $0.47\mu\text{m}$ (3σ) by measuring the displacement between the two PZSs with the high-precision laser displacement sensors and controlling one PZS (the other PZS was used for disturbance input). This single-axis control experiment was emulated in a software simulation, which has numerical models of the components constructed from the experiments. The similar process of verifying the μm -class control by the hardware experiments and confirming the validity of the numerical models by emulating the experimental results in software simulation was also performed in the 3-axis control experiment. Furthermore, the μm -class formation flying control of the entire FFSAT system was simulated by using a simulator integrating the numerical models. The results of the simulation, highly accurate control was achieved with dual-stage actuators, which consist of the PZSs and the cold gas thrusters. The achieved control accuracy is less than μm order, which is sufficiently smaller than the assumed observation wavelength of $4\mu\text{m}$, and we think the residual control errors can be removed by adaptive optics using deformable mirrors. We also think that the space environment resistance of the components used in the experiments is important, and we will continue to evaluate it in the future.

In addition, the use of the FFSAT is not limited to GEO remote sensing. The FFSAT theoretically has no upper limit on its aperture diameter. The FFSAT has the possibility to realize much larger aperture diameter and to achieve much higher spatial resolution compared with conventional space telescopes. By applying the FFSAT to an astronomical observation telescope, an unprecedented observation such as a direct observation of extrasolar planets will be possible. For that purpose as well, it is necessary to need to continue studying for the realization of the FFSAT in the future.

REFERENCES

- Armano, M., Audley, H., Baird, J., Binetruy, P., Born, M., Bortoluzzi, D., Castelli, E., Cavalleri, A., Cesarini, A., Cruise, A.M., Danzmann, K., de Deus Silva, M., Diepholz, I., Dixon, G., Dolesi, R., Ferraioli, L., Ferroni, V., Fitzsimons, E.D., Freschi, M., Gesa, L., Gibert, F., Giardini, D., Giusteri, R., Grimani, C., Grzymisch, J., Harrison, I., Heinzl, G., Hewitson, M., Hollington, D., Hoyland, D., Hueller, M., Inchauspé, H., Jennrich, O., Jetzer, P., Karnesis, N., Kaune, B., Korsakova, N., Killow, C.J., Lobo, J.A., Lloro, I., Liu, L., López-Zaragoza, J.P., Maarschalkerweerd, R., Mance, D., Meshksar, N., Martín, V., Martín-Polo, L., Martino, J., Martín-Porqueras, F., Mateos, I., McNamara, P.W., Mendes, J., Mendes, L., Nofrarias, M., Paczkowski, S., Perreur-Lloyd, M., Petiteau, A., Pivato, P., Plagnol, E., Ramos-Castro, J., Reiche, J., Robertson, D.I., Rivas, F., Russano, G., Slutsky, J., Sopena, C.F., Sumner, T., Texier, D., Thorpe, J.I., et al. (2019). LISA Pathfinder micronewton cold gas thrusters: In-flight characterization. *Physical Review D*, 99(12), 122003.
- Bandyopadhyay, S., Foust, R., Subramanian, G.P., Chung, S.J., and Hadaegh, F.Y. (2016). Review of Formation Flying and Constellation Missions Using Nanosatellites. *Journal of Spacecraft and Rockets*, 53(3), 567–578.
- D’Amico, S., Koenig, A., Macintosh, B., and Mauro, D. (2019). System Design of the Miniaturized Distributed Occulter/Telescope (mDOT) Science Mission. *33rd Annual AIAA/USU Conference on Small Satellites*, SSC19-IV-08.
- Gath, P.F., Fichter, W., Kersten, M., and Schleicher, A. (2004). Drag Free and Attitude Control System Design for the LISA Pathfinder Mission. *AIAA Guidance, Navigation, and Control Conference and Exhibit*, AIAA 2004-5430.
- Holden, B., Morgan, R., Allan, G., Pereira, P.d.V., Grunwald, W., Gubner, J., Haughwout, C., Stein, A., Xin, Y., Cahoy, K., Douglas, E., Merk, J., Egan, M., and Furesz, G. (2019). Calibration and Testing of the Deformable Mirror Demonstration Mission (DeMi) CubeSat Payload. *33rd Annual AIAA/USU Conference on Small Satellites*, SSC19-WKIV-03.
- Hutchison, K.D. (2003). Applications of MODIS satellite data and products for monitoring air quality in the state of Texas. *Atmospheric Environment*, 37, 2403–2412.
- Miyamura, N., Suzumoto, R., Mori, D., Funabiki, N., Matsushita, S., Ikari, S., Kawabata, Y., and Nakasuka, S. (2019). Conceptual Optical Design of a Synthetic Aperture Telescope by Small Satellite Formation Flying for GEO Remote Sensing. *32nd International Symposium on Space Technology and Science*, 2019-f-59.
- Rousset, G., Mugnier, L., Cassaing, F., and Sorrente, B. (2001). Imaging with multi-aperture optical telescopes and an application. *OPTICAL INTERFEROMETRY AT GROUND LEVEL AND IN SPACE*, 2(1), 17–25.
- Scharf, D.P., Hadaegh, F.Y., Rahman, Z.H., Shields, J.F., Singh, G., and Wette, M.R. (2004). An Overview of the Formation and Attitude Control System for the Terrestrial Planet Finder Interferometer. *The 2nd International Symposium on Formation Flying Missions and Technologies*, NASA/CP-2005-212781.
- Smith, M.W., Donner, A., Knapp, M., Pong, C.M., Smith, C., Luu, J., Pasquale, P.D., Bocchino, R.L., Campuzano, B., Loveland, J., Colley, C., Babuscia, A., White, M., Krajewski, J., and Seager, S. (2018). On-Orbit Results and Lessons Learned from the ASTERIA Space Telescope Mission. *32nd Annual AIAA/USU Conference on Small Satellites*, SSC18-I-08.
- Suzumoto, R., Ikari, S., Miyamura, N., and Nakasuka, S. (2019). Accurate Control of Relative Position and Attitude for Formation Flying Synthetic Aperture Telescope with Multiple Micro-satellites. *32nd International Symposium on Space Technology and Science*, 2019-n-41s.
- Tatebatake, K., Ueda, Y., Liu, D., and Fujii, F. (2017). Modeling of hysteresis characteristics of the piezoelectric actuator using the bouc-wen model. *Transactions of the JSME*, 83(852).